Science of the Total Environment 839 (2022) 155941

Contents lists available at ScienceDirect

Science of the Total Environment

journal homepage: www.elsevier.com/locate/scitotenv

Modelling of the photo-Fenton process with flexible hydrogen peroxide dosage: Sensitivity analysis and experimental validation

Kourosh Nasr Esfahani, Montserrat Pérez-Moya *, Moisès Graells

Chemical Engineering Department, EEBE, Universitat Politècnica de Catalunya, Av. Eduard Maristany, 16, 08019 Barcelona, Spain

HIGHLIGHTS

- A photo-Fenton treatment model is proposed including variable H_2O_2 dosage.
- Model parameters are checked and reduced according to sensitivity analysis.
- Parameters are fit to experimental data sets with diverse H_2O_2 dosage profiles.
- Successful model validation is finally obtained using out-of-sample testing.

GRAPHICAL ABSTRACT

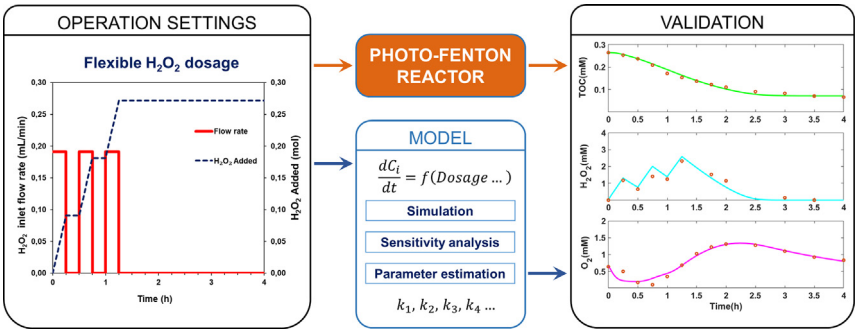

ARTICLE INFO

Editor: Paola Verlicchi

Keywords:
Photo-Fenton process
Dosage of hydrogen peroxide
Mathematical modelling
Model fitting
Parameter estimation
Sensitivity analysis
Validation

ABSTRACT

The supply of hydrogen peroxide (H_2O_2) controlling the amount of highly oxidant hydroxyl radicals is the most critical operational issue for the photo-Fenton process. Accordingly, this study addresses the development of a model for photo-Fenton processes including a flexible H_2O_2 supply given as a function of time. The model is aimed at its future exploitation in treatment optimization and the determination of the optimal profile for H_2O_2 supply. The work has adopted a photo Fenton model previously reported that includes the inlet flow (fed-batch) and describes the system dynamics under a flexible dosage. Thus, model global sensitivity analysis (GSA) and parameter estimation were performed using Simulink® to examine the behavior of the model under flexible H_2O_2 dosage. GSA was carried out using partial rank correlation methods and the Latin hypercube sampling to assess to which extent variations of the model parameters affect each measured response (H_2O_2, total organic carbon, TOC, and dissolved oxygen, O_2 –the experimentally available information). Hence, the model is discussed in regard of its hypothesis and chances for reducing its complexity. This resulted in the rejection of two reactions of the initial model. Next, a set of 12 kinetic, stoichiometric and operative parameters was estimated through the fitting of H_2O_2, TOC, and O_2 profiles. Discussion on model fitting includes computational issues, the role of initial values for the estimation process, the goodness of fit criteria, and the sampling method. The model was fit to experimental data with assorted H_2O_2 supply profiles and validated, and Root Mean Square Error (RMSE) below 0.009 mM, 0.42 mM, and 0.127 mM were obtained for TOC, H_2O_2 and O_2, respectively. Therefore, this work contributes a practical model aimed at providing model-based optimization for the H_2O_2 dosage profile of the photo-Fenton process.

1. Introduction

The presence of many non-biodegradable organic pollutants in wastewaters or surface waters (including industrial compounds, pharmaceuticals, personal-care products, biocides, and plant protection substances) may result in important environmental issues even in very low

* Corresponding author.
E-mail address: montserrat.perez-moya@upc.edu (M. Pérez-Moya).

http://dx.doi.org/10.1016/j.scitotenv.2022.155941
Received 23 March 2022; Received in revised form 6 May 2022; Accepted 10 May 2022
Available online 14 May 2022

concentrations. Ineffective treatment of the organic pollutants in wastewaters, as well as the direct release of them into the environment, may lead to the infiltration of profoundly poisonous and low biodegradable species into the natural aquatic ecosystems.

Several treatment techniques including both physicochemical and biological methods could be applied to contaminated wastewaters. In any case, few strategies are adequately broad-based and helpful for real-time applications (Lu et al., 2011; Oller et al., 2011).

Advanced oxidation processes (AOPs) have been broadly acknowledged as promising strategies either individually or in combination for the remediation of contaminated wastewaters containing non-biodegradable organic pollutants (Tufail et al., 2020).

Among these processes, the photo Fenton treatment is a well-known solution for treating non-biodegradable contaminants in wastewaters that cannot be treated with conventional bio-processes (Oller et al., 2011). It has gotten a lot of interest because of its broad range of target chemicals, robust oxidation capabilities, and rapid response pace (Lu et al., 2010).

The photo-Fenton process is a photocatalytic process that generates highly oxidizing hydroxyl radicals (•OH) by interacting chemical reagents (Fe (II) salt and H_2O_2) with a UV irradiation light source, which causes a synergic effect by creating a higher rate of •OH production.

However, the major limitations of this method are the need for H_2O_2, Fe^{+2} salts and pH adjustment (mostly acidic)(Lu et al., 2010; Pignatello et al., 2006). Furthermore, the hydroxyl radical is exceedingly unstable and non-selective, so it is frequently scavenged by unwanted secondary reactions, some of them involving H_2O_2 consumption, which cut down the efficiency of the process (Gulkaya et al., 2006).

Hence, it is critical to control the reaction conditions through the dosage of H_2O_2 for achieving the complete mineralization of the target compound, i.e. The reaction rate and process efficiency are both affected by H_2O_2, which is the most expensive reagent (Lu et al., 2011). This represents a compromise between decontamination efficiency of the process due to H_2O_2 deficiency and excess concentration of H_2O_2 that forces extra cost. In this regard, researchers have studied the photo-Fenton process with the dosage of Hydrogen peroxide to enhance process performance (Santos-Juanes et al., 2011)

As a straightforward approach for the supply of hydrogen peroxide, constant concentration ratios of H_2O_2 to contaminant and iron were studied to minimize the scavenging effect (Gulkaya et al., 2006; Mahmoudi et al., 2021; Sinnaraprasat and Fongsatitkul, 2011). While such ratios may suit steady operation, time-varying batch operations may require constantly adapted H_2O_2 supply to optimize the operation performance (Yu et al., 2020). As a result, the key research issue is the optimization of a time-dependent H_2O_2 dose profile to maximize process performance by reducing the scavenging effects through the supply of the required amount of hydrogen peroxide supply at all times.

Towards this end, Ortega-Gómez et al. (2012) investigated a control strategy for the automatic addition of hydrogen peroxide and the linking behavior of dissolved oxygen to hydrogen peroxide consumption. It was demonstrated that, through the application of this control strategy, the hydrogen peroxide consumed can be reduced by 50% compared to the more traditional addition strategies employed in the photo-Fenton process (Ortega-Gómez et al., 2012). More recently, Yu et al. (2020) presented a conceptual basis and an experimental approach to address the problem of hydrogen peroxide dosage for Fenton and photo-Fenton processes. The mineralization was further improved in a specific H_2O_2 dosage (by 4.75%) rather than the same amount of hydrogen peroxide without dosage (Yu et al., 2020).

Whereas most of the previous experimental works verified an increase in the photo Fenton process efficiency using flexible dosage strategies (Hamad et al., 2016; Yamal-Turbay et al., 2014; Yu et al., 2020), they are useful in particular situations and cannot provide the optimal solution.

On the other hand, despite some attempts proposing different models for hydrogen peroxide dosage in the Fenton based processes (Audino et al., 2019a; Bacardit et al., 2007), solutions reported in the literature are still incomplete and fall short of offering a dynamic model of batch and fed-batch operations of the photo Fenton process using systematic approaches.

Furthermore, the computational costs associated with developing a comprehensive model can be a limiting factor in terms of model parameter estimation and sensitivity analysis. Several studies with sensitivity analysis have been performed for the Fenton-based processes and it has been confirmed the usefulness of the different kinetic reactions, especially the scavenging reactions to be considered (Căilean et al., 2015; Mousset et al., 2016). Still, based on the different range of parameter values found in the literature (Shinozawa et al., 2020), it is necessary to study kinetic parameter estimations and sensitivity analysis for each specific model in order to better fit the experimental results.

In other words, the lack of suitable dynamic models for Fenton and photo-Fenton processes makes model-based optimization challenging, and determining the optimum hydrogen peroxide supply profile has been hardly addressed (Audino et al., 2019a). In fact, scarce attention has been paid to the development of systematic procedures and optimization strategies to efficiently operate the photo Fenton process including flexible dosage.

The rigorous model-based optimization of the dosage profile is beyond the scope of the present work. The target is determining a continuous function for the dosage level to be applied at each differential time step so that any given cost function (economic, environmental, etc.) is minimized at the end of the dosage. However, in order to address such a dynamic optimization problem, a dynamic model is first required allowing the estimation of the evolution of the outcome of the process (i.e. TOC) from a time-controlled input (i.e. the H_2O_2 dosage profile). The objective and scope of this work are shedding new light on the dosage problem and the development and fitting to experimental data of a practical photo-Fenton model including flexible H_2O_2 dosage. This work is a necessary step towards solving the model-based optimization problem, which is not immediate and would require further research.

The work follows and extends the approach by Cabrera Reina et al. (2012) and Audino et al. (2019a) to model a time-dependent supply of hydrogen peroxide to a batch reactor, and uses the experimental data obtained by Yu et al. (2020) using different dosage schemes for the mineralization of paracetamol solutions at a pilot plant scale.

Thus, sensitivity analysis is the first step allowing balancing the complexity and the accuracy of the model. Next, the model is fit to different sets of experimental data and validated using new data (cross-validation). Finally, the precision and accuracy of the model are discussed in regard to its potential for addressing the optimization of a continuous time-dependent H_2O_2 dosage profile that would in turn support informed decision-making on the H_2O_2 supply problem in photo-Fenton treatments.

2. Methodology

The proposed methodology consists of the simulation of the model for a variable operation of the reactor with different H_2O_2 supply, sensitivity analysis, parameter estimation using experimental data, and final validation with the evaluation of the results for the practical applications. The flow diagram of the methodological framework followed is illustrated in Fig. 1.

Accordingly, this section describes and discusses the model adopted and its implementation in Simulink® (Section 2.1); the data used to calibrate and validate the model (Section 2.2) the methods employed for the quantitative assessment of the fidelity of the model, and the sensitivity of its output to model parameters (Section 2.3); and the procedure to use this information to assess and discuss its consistency and complexity through sensitivity analysis (Section 2.4). Finally, Section 3 presents and discusses the results obtained.

Simulations and analysis of the model are proposed with the ultimate goal of verifying the model implementation and learning from the different computational experiments that can be produced. Next, global sensitivity analysis is intended for assessing to which extent variations of the model parameters affect each measured response (TOC, H_2O_2, and O_2) with a

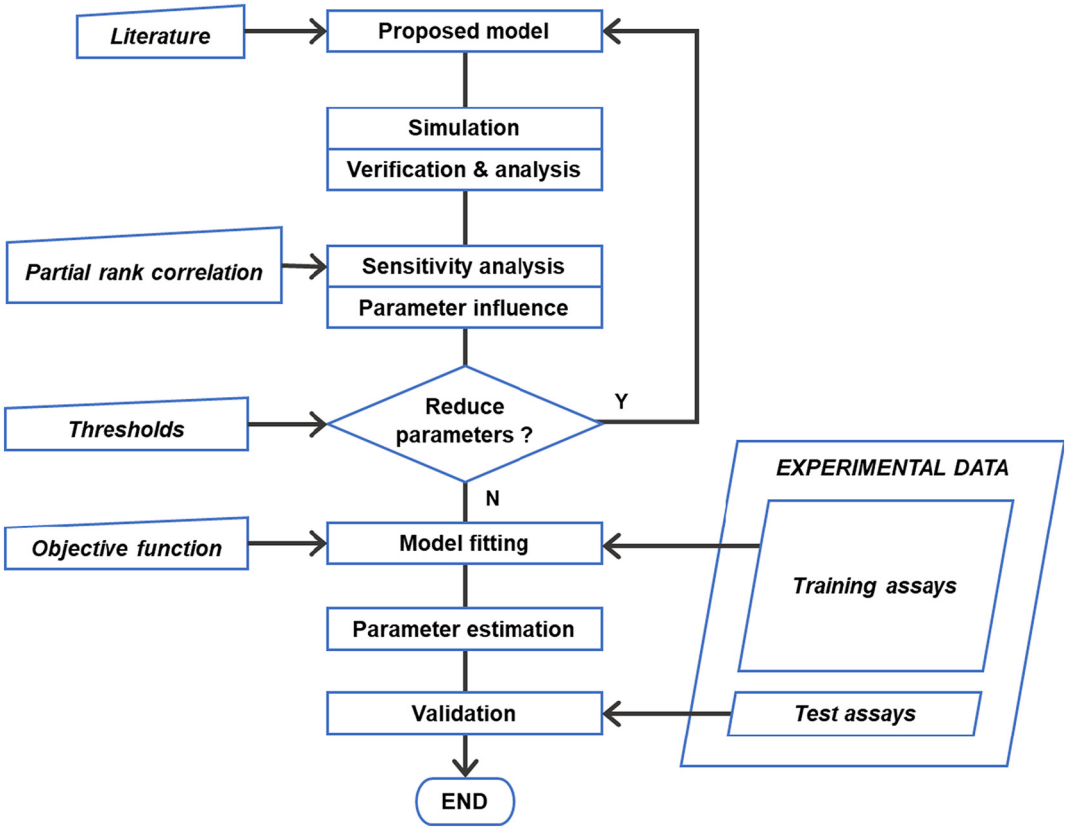

Fig. 1. Methodological framework.

quantified correlation coefficient for each parameter. Thresholds are established and discussed. Results in Section 3.2 reveal non-significant parameters that are eliminated as their absolute correlation coefficients below 0.10 for TOC, H_2O_2, and O_2 (the experimentally available information).

Parameter estimation is proposed through the minimization of the sum of the squared differences between the model values and the training data (88% of the experimental assays). Finally, validation is proposed by assessing the capacity of the fitted model to explain independent experimental data sets not used in the calibration of the model (test assays).

2.1. Mathematical modelling and simulation

The photo-Fenton process model adopted is based on that by Cabrera Reina et al. (2012) and later extended by Audino et al. (2019a) to include

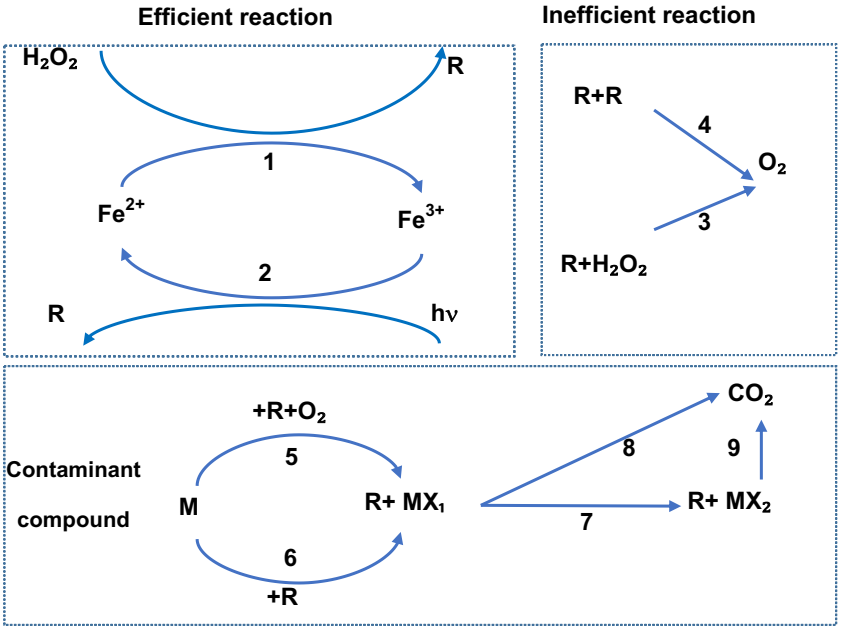

Fig. 2. The reaction scheme of the photo Fenton model according to Cabrera Reina et al. (2012).

flexible dosage via fed-batch operation. The reaction scheme is given in Fig. 2.

The formation of hydroxyl radicals is described through efficient reactions (Eqs. (1) and (2)) between Iron (II) and hydrogen peroxide (H_2O_2), as well as efficient reactions between the resulting Iron (III) and UV irradiation. The low pH requirement (between 3 and 6) is assumed, as usual, as an important condition for iron-induced reduction of hydrogen peroxide. In the same way, a convenient light source with a proper constant wavelength (nm) is assumed and not included in the model; thus, the model is limited to the specific wavelength used. Contrariwise, the model does contemplate light intensity [*I*] and it can be fitted to the experimental data, but again the model will be limited, this time because all the experimental data used are obtained under constant irradiation.

$$r_1 = k_1.[Fe^{2+}][H_2O_2] \tag{1}$$

$$r_2 = k_2.[Fe^{3+}][I] \tag{2}$$

Radicals R decompose H_2O_2 (Reaction (3)) and combine (Reaction (4)) producing oxygen in both cases. Thus, an excess of H_2O_2 and radicals can go through these inefficient paths instead of being used in the oxidation of the organic matter M.

The existence and propagation of any of these reactions highly depend on the amount of H_2O_2 as well as the rate constant. It's also worth noting that increasing the hydrogen peroxide concentration lowers the process efficiency because it raises the concentration of radicals [*R*].

$$r_3 = k_3.[R][H_2O_2] \tag{3}$$

$$r_4 = k_4.[R][R] \tag{4}$$

The model also assumes the consumption of radicals R in a series of oxidations leading the parent compound M to the partially oxidized intermediates MX_1 and MX_2, and finally to CO_2 (Reactions (5)–(9)). The concentrations of three species determine the measurement of Total Organic Carbon (TOC = M + MX_1 + MX_2) and allow modelling the delayed response of such a lumped parameter.

Reactions (5) and (6) are associated with the degradation of the main organic matter to produce MX_1 and then MX_2 by means of Reaction (7). Finally, the degradation of the intermediates is modelled through Reactions (7) to (9).

$$r_5 = k_5.[M][R][O_2] \tag{5}$$

$$r_6 = k_6.[M][R] \tag{6}$$

$$r_7 = k_7.[MX_1][R] \tag{7}$$

$$r_8 = k_8.[MX_1][R] \tag{8}$$

$$r_9 = k_9.[MX_2][R] \tag{9}$$

The mass balance equations, including the overall gas-liquid mass transfer coefficient for O_2 (K_La) and the stoichiometric coefficients related to the oxygen balance (c_1, g_1, and g_2), are shown below (Eqs. (10)–(18)):

$$\frac{d[H_2O_2]}{dt} = \left(\frac{F}{V}\right)\bullet\left([H_2O_2]_{in} - [H_2O_2]\right) - r_1 - r_3 \tag{10}$$

$$\frac{d[M]}{dt} = \left(\frac{F}{V}\right)\bullet\left([M]_{in} - [M]\right) - r_5 - r_6 \tag{11}$$

$$\frac{d[MX_1]}{dt} = \left(\frac{F}{V}\right)\bullet\left([MX_1]_{in} - [MX_1]\right) + r_5 + r_6 - r_7 - r_8 \tag{12}$$

$$\frac{d[MX_2]}{dt} = \left(\frac{F}{V}\right)\bullet\left([MX_2]_{in} - [MX_2]\right) + r_7 - r_9 \tag{13}$$

$$\frac{d[TOC]}{dt} = \frac{d[M]}{dt} + \frac{d[MX_1]}{dt} + \frac{d[MX_2]}{dt} \tag{14}$$

$$\frac{\mathrm{d}[O_2]}{\mathrm{dt}} = \left(\frac{F}{V}\right)\bullet\left([O_2]_{in} - [O_2]\right) + g_1r_3 + g_2r_4 - c_1r_5 + \left(K_La([O_2]^* - [O_2])\right) \tag{15}$$

$$\frac{d\left[Fe^{2+}\right]}{dt} = \left(\frac{F}{V}\right)\bullet\left(\left[Fe^{2+}\right]_{in} - \left[Fe^{2+}\right]\right) - r_1 + r_2 \tag{16}$$

$$\frac{d\left[Fe^{3+}\right]}{dt} = \left(\frac{F}{V}\right)\bullet\left(\left[Fe^{3+}\right]_{in} - \left[Fe^{3+}\right]\right) + r_1 - r_2 \tag{17}$$

$$\frac{d[R]}{dt} = \left(\frac{F}{V}\right)\bullet\left([R]_{in} - [R]\right) + r_1 + r_2 - r_3 - 2r_4 - r_5 - r_6 - r_7 - r_8 - r_9 \tag{18}$$

where *F*, represents the inlet flow rate ($L.h^{-1}$); *V* (*L*), the total volume of the reactor and $[C_i]_{in}$ as well as $[C_i]$ refer to the concentrations ($mmol.L^{-1}$) for each component in the inlet flow rate and inside the reactor, respectively. In this particular study, all inlet concentrations are considered null except $[H_2O_2]_{in}$.

Hence, the model parameters of the photo Fenton process model to be considered are k_1 to k_9, K_La, and the stoichiometric coefficients c_1, g_1, and g_2.

The model is based on the main following assumptions (Audino et al., 2019a):

I. The different radical species that may exist are represented by their aggregated concentration [*R*] and common behavior.
II. The reaction between Fe^{3+} and H_2O_2 is neglected so that the model is only applicable to the photo Fenton process (UV light is necessary);
III. H_2O_2 hydrolysis is neglected;
IV. An intermediate partially oxidized compound is assumed to be present before any CO_2 is released from the process.

The main features of the model include the focus on parameters easy to monitor such as dissolved oxygen, hydrogen peroxide, and TOC; the use of unspecified intermediates (MX_1, MX_2, as artificial, dummy variables) to model the delay in the response of this practical lumped measurement; and the easy modelling of the scavenging of H_2O_2 by means the non-linear consumption of radicals (Eqs. (3) and (4)).

The model given by the set of Ordinary Differential Equations (Eqs. (10) to (18)) is implemented in MATLAB/Simulink® version R2021b and solved numerically using ode15s solver as a variable order solver based on the numerical differentiation formulas with a time variable-step.

Fig. 3 illustrates the capability of describing the evolution of the concentration of all the components included in the simulation of the kinetic model. The normalized values are calculated according to unity-based normalization as shown in Eq. (19):

$$Normalized\ C_i = \frac{C_i - C_{min}}{C_{max} - C_{min}} \tag{19}$$

Table 1 provides the data given by Cabrera Reina et al. (2012) used for the simulations shown in Fig. 4 (as mentioned, only $[H_2O_2]_{in}$ is different from zero, while the rest of inlet concentrations are null).

The simulation example corresponds to a variable of H_2O_2 dosage profile stemming from a flow rate of 0.143 ($mL \cdot min^{-1}$) that is switched on from 0 to 15 min and from 30 to 75 min (Fig. 3a). These operational settings will produce an experimentally monitored response (TOC, H_2O_2 and O_2) displayed in Fig. 3b. Furthermore, simulation provides deeper insight into the process by revealing the concentration of intermediates and other unobservable species: the profiles of M, MX_1, MX_2show the successive transformation of M to $MX_1$and to MX_2, with both intermediates peaking at early reaction times and gradually declining as the mineralization progresses (Fig. 3c). As a result, TOC remains unaltered for a short time and then asymptotically decreases, exhibiting a delayed response. The simulated

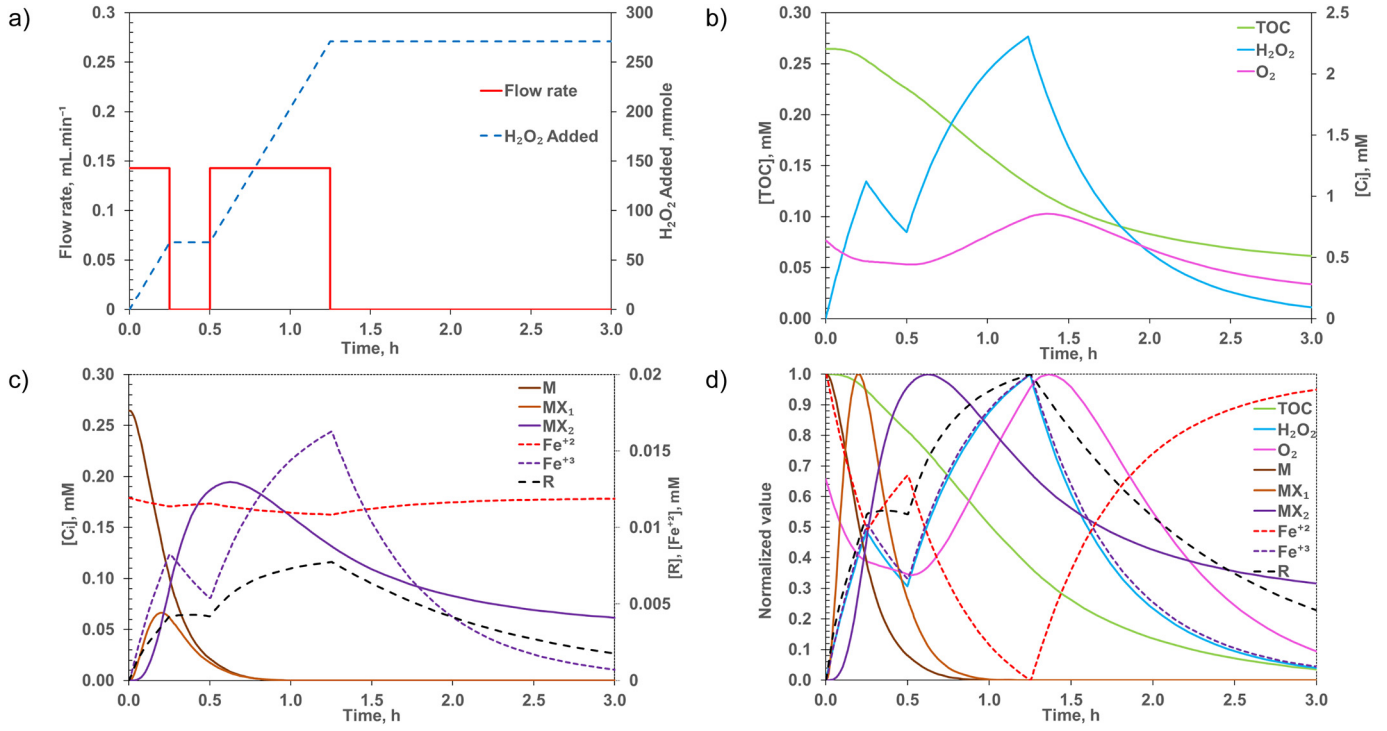

Fig. 3. Simulation of concentration profiles: (a) Variable H_2O_2 input profile: a constant flow rate (0.14318 mL · min^{-1}) is kept from 0 to 15 min and from 30 to 75 min; totaling (8.5909 mL, 271.29 mmol) at the end of the 3 h reaction time simulated; (b) Concentration profiles of the measured output: TOC, H_2O_2, O_2; (c) Concentration profiles (absolute values) for organic species (M, MX_1, MX_2), radicals (R), and iron species (Fe^{2+}, Fe^{3+}); (d) Concentration profiles for all species (normalized values).

profile of dissolved oxygen concentration shows a correspondence with the levels of both H_2O_2 and R and also supports the idea that dissolved oxygen may indicate an unproductive decomposition of hydrogen peroxide that should be avoided. Finally, Fig. 3d presents the concentrations of all species using normalized values for comparative purposes. Fig. 3d clearly shows the parallel evolution of hydrogen peroxide and iron and the delayed response of the radical species R respect to the concentration of H_2O_2.

2.2. Experimental data

The experimental data used to calibrate the model is also obtained from the literature (Yu et al., 2020). The work by Yu et al. (2020) addresses the formulation of the optimization of a fully flexible H_2O_2dosage profile in photo-Fenton processes and reports data series according to this idea. The work is limited because of the unaffordable experimental burden but stresses the need for a reliable process model and provides suitable data for calibrating such a model.

The work by Yu et al. (2020) specifically studied the photo-Fenton remediation of a Paracetamol (PCT) and the experimental results include the evolution of the concentration of TOC, H_2O_2, and O_2. The data reported corresponds to a set of systematically designed dosage profiles covering a complete domain of alternatives (Table 2). The reaction time (2 h) was divided into eight-time slots of 15 min (S1 to S8) and for each one dosage was set active or not (1,0) so that the same amount of H_2O_2 was fractioned and distributed along such time span.

For all profiles, the first slot (S1) is obviously always on (1), while for the last three (S6, S7, and S8) dosage was decided to be off (0). Thus, there are four degrees of freedom (S2, S3, S4, and S5, shadowed in Table 2) and 16 cases leading to the codification used in Table 2. The label "No dosage" refers to the assay for which the same total amount of H_2O_2 was supplied all at once at the beginning, and for which this codification does not apply (N/A).

In order to illustrate the design of experiments, three cases (Code 02, Code 05, and Code 07) are represented in Fig. 4, showing each dosage profile set and the corresponding response obtained (TOC, H_2O_2, and O_2). All experiments were repeated twice, and the average values are represented and used as reported by Yu et al. (2020).

2.3. Model fitting and parameter estimation

The model (Eqs. (1)–(18)) is calibrated by estimating the best parameter values. This is done by solving a nonlinear multivariate optimization problem to minimize the sum of the squared differences between the model values and the corresponding experimental data available. In this case, this includes the easily monitored TOC, H_2O_2, and O_2 concentrations, while excluding dummy variables such as the concentrations of intermediates (MX_1, MX_2, etc.). This is summarized by Eq. (20).

$$min\ Z = \sum_i \left(\widehat{[TOC]}_i - [TOC]_i \right)^2 + \sum_j \left(\widehat{[H_2O_2]}_j - [H_2O_2]_j \right)^2 + \sum_k \left(\widehat{[O_2]}_k - [O_2]_k \right)^2 \quad (20)$$

where the circumflex denotes experimental data.

Table 1
Model parameters and initial concentrations (Cabrera Reina et al., 2012).

Kinetic constants	Value	Initial concentrations	Value
$K_La(h^{-1})$	2.7	$[H_2O_2]_0$ (mM)	0
c_1	0.1	$[TOC]_0$ (mM)	0.26
g_1	0.75	$[O_2]_0$ (mM)	0.64
g_2	0.47	$[Fe^{2+}]_0$ (mM)	0.179
$k_1(mM^{-1}.h^{-1})$	8.81	$[Fe^{3+}]_0$ (mM)	0
$k_2((W.m^{-2})^{-1}.h^{-1})$	5.63	$[M]_0$ (mM)	0.26
$k_3(mM^{-1}.h^{-1})$	75.8	$[MX_1]_0$ (mM)	0
$k_4(mM^{-1}.h^{-1})$	42,798	$[MX_2]_0$ (mM)	0
$k_5(mM^{-2}.h^{-1})$	2643	$[R]_0$ (mM)	0
$k_6(mM^{-1}.h^{-1})$	257	$[O_2]^*$ (mM)	0.21
$k_7(mM^{-1}.h^{-1})$	2865	I (W. m^{-2})	36
$k_8(mM^{-1}.h^{-1})$	271	F(ml. min^{-1})	0.143
$k_9(mM^{-1}.h^{-1})$	107	Total volume, V (L)	15

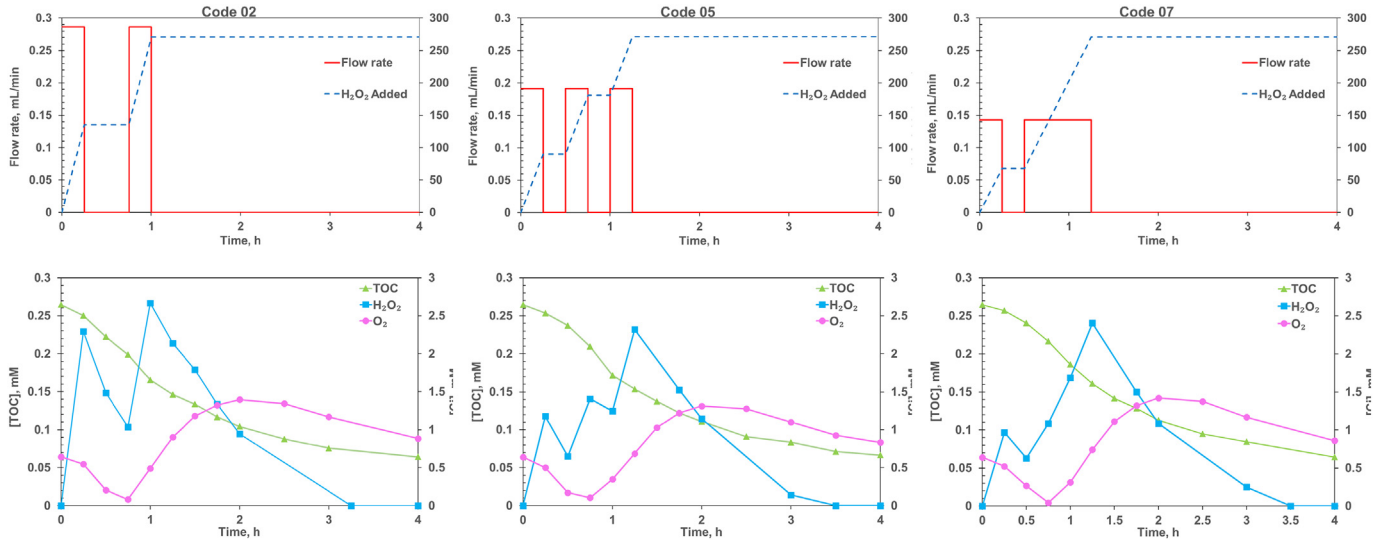

Fig. 4. Experimental data for 3 particular hydrogen peroxide dosage profiles (codes 2, 5, and 7; 4 h reaction time). Above: flow rate and amount of H_2O_2 added. Below: TOC, H_2O_2 and O_2evolution.

This problem is solved using the Non-linear least-squares method with the Levenberg-Marquardt algorithm available in the Estimator Toolbox of MATLAB/Simulink® version R2021b.

To assess the goodness of fit, the Root Mean Square Error (RMSE), as the standard deviation of the residuals (prediction errors), will be used and presented for each measured time series k (TOC, H_2O_2, and O_2, -Eq. (21)). The coefficient of determination R^2 (Eq. (22)) is also presented as an informative statistical measure that is widely used. Caution is required in the use and interpretation of R^2 in nonlinear models since the total sum-of-squares is not equal to the regression sum-of-squares plus the residual sum-of-squares, as in the case of linear regression (Spiess and Neumeyer, 2010). It is used along with RMSE for illustrative purposes.

$$RMSE_k = \sqrt{\left(\sum_{i=1}^{N_k} (\hat{y}_{ik} - y_{ik})^2 / N_k\right)} \tag{21}$$

$$R_k{}^2 = 1 - \left(\sum_{i=1}^{N} (\hat{y}_i - y_i)^2 / \sum_{i=1}^{N} (\hat{y}_i - \bar{y})^2\right) \tag{22}$$

where $\hat{y}_i$ and y_i correspond to the measured and simulated values at the given time, respectively, and $\bar{y}$ is the mean of the measured data.

Table 2
Design of experiments (Yu et al., 2020).

ID (Code)	ID (bin)	S1	S2	S3	S4	S5	S6	S7	S8	Fraction per slot
No dosage	N/A	N/A	N/A	N/A	N/A	N/A	N/A	N/A	N/A	N/A
0	**0000**	1	**0**	**0**	**0**	**0**	0	0	0	1
1	**0001**	1	**0**	**0**	**0**	**1**	0	0	0	1/2
2	**0010**	1	**0**	**0**	**1**	**0**	0	0	0	1/2
3	**0011**	1	**0**	**0**	**1**	**1**	0	0	0	1/3
4	**0100**	1	**0**	**1**	**0**	**0**	0	0	0	1/2
5	**0101**	1	**0**	**1**	**0**	**1**	0	0	0	1/3
6	**0110**	1	**0**	**1**	**1**	**0**	0	0	0	1/3
7	**0111**	1	**0**	**1**	**1**	**1**	0	0	0	1/4
8	**1000**	1	**1**	**0**	**0**	**0**	0	0	0	1/2
9	**1001**	1	**1**	**0**	**0**	**1**	0	0	0	1/3
10	**1010**	1	**1**	**0**	**1**	**0**	0	0	0	1/3
11	**1011**	1	**1**	**0**	**1**	**1**	0	0	0	1/4
12	**1100**	1	**1**	**1**	**0**	**0**	0	0	0	1/3
13	**1101**	1	**1**	**1**	**0**	**1**	0	0	0	1/4
14	**1110**	1	**1**	**1**	**1**	**0**	0	0	0	1/4
15	**1111**	1	**1**	**1**	**1**	**1**	0	0	0	1/5

2.4. Global sensitivity analysis

Parameter sensitivity analysis is used to examine a mathematical model to reveal the relative importance of the various mechanisms included in the model and the robustness of its output with respect to parameter uncertainty (Latunde and Bamigbola, 2018).

One approach to sensitivity analysis is Local Sensitivity Analysis (LSA), which is computationally inexpensive. They are based on derivatives (numerical or analytical) and analyze the effect of one parameter at a time, while the other parameters are kept constant. However, these methods are limited to the exploration of only a small portion of the solution space (Castillo et al., 2004).

Another approach is global sensitivity analysis (GSA), often implemented using Monte Carlo techniques to overcome the limits of LSA (linearity and normality assumptions and local variations). GSA uses a globally representative set of samples to explore the solution space. Furthermore, several input factors can be simultaneously varied to evaluate not only the effect of one factor at a time but also the effect of interactions between inputs, since the sensitivity to an input may depend on other inputs (Saltelli et al., 1999). In this study, GSA is adopted as it has been implemented frequently for models having multiple correlated outputs.

There are several GSA techniques, mostly statistical and analytical methods. New analytical and statistical methods are reported such as global screening methods (e.g. Morris method)(Campolongo et al., 2007), variance-based methods (e.g. Sobol's method and Fourier Amplitude Sensitivity Test) (Saltelli et al., 1999) sampling-based methods (e.g. Latin hypercube sampling with partial rank correlation coefficient index, LHS-PRCC) (Helton et al., 2006) and others. These techniques have been developed specifically for complex models of policy and allocation problems.

One of the statistical methods for GSA using the sampling techniques is the application of partial rank correlation coefficients (PRCC) as a measure of sensitivity for a large, complex computerized model. The best of the sampling schemes, Latin hypercube sampling (LHS), is a procedure that structures input trials in an optimum and comprehensive model-testing design. The LHS method is selected along with an efficient stratification Monte Carlo sampling method allowing the extraction of a large amount of uncertainty and sensitivity information with a relatively small sample size (Marino et al., 2008).

The combined LHS-PRCC method is used to analyze how the model parameters and the output are correlated, removing the effects of the remaining parameters and considering general monotonic relationships between inputs and outputs. In PRCC, also referred to as Spearman analysis and

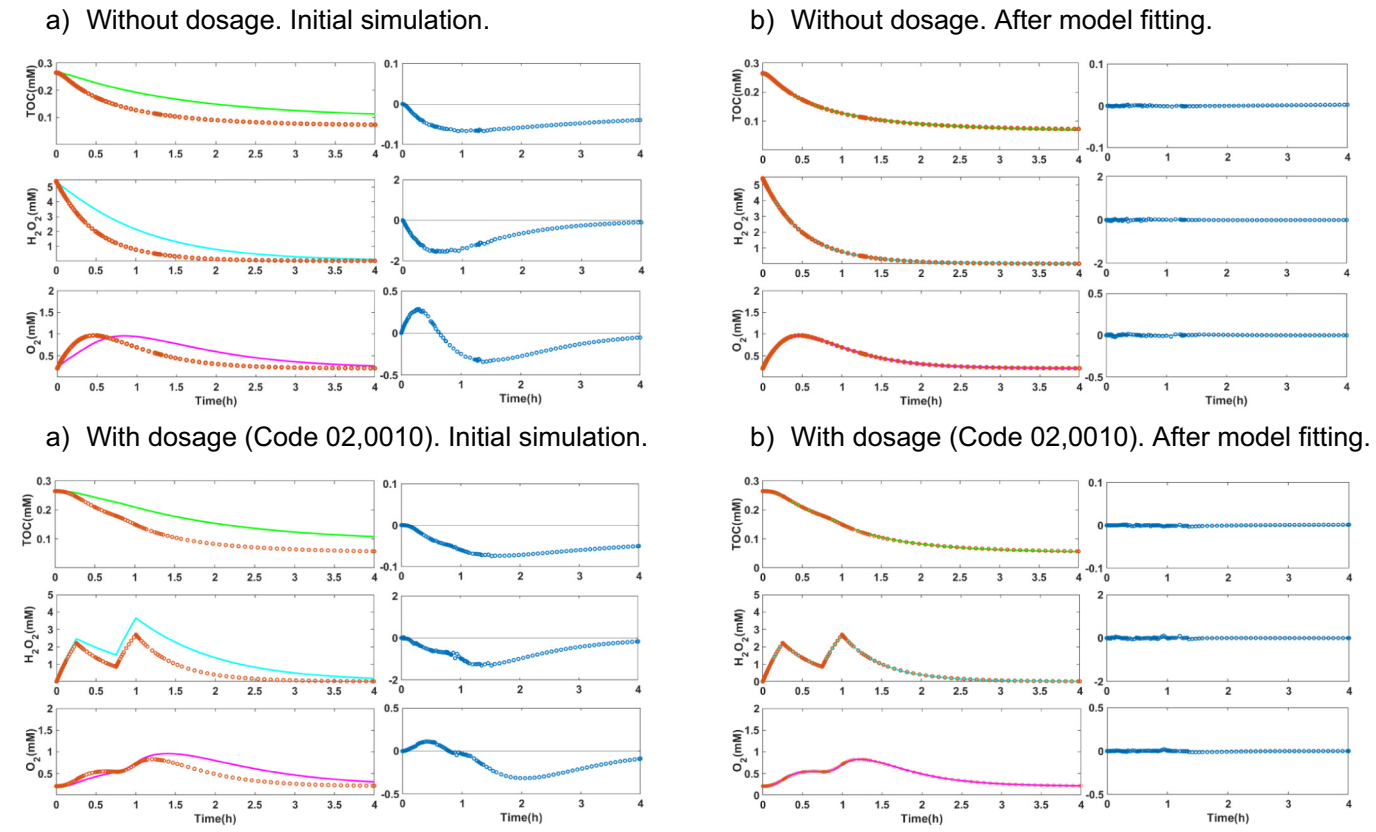

Fig. 5. Parameter estimation and residual values for two illustrative cases with and without dosage (simulated data).

ranked transformation, a model with P number of model parameters and a model output y can be written as a function of all the model parameters values x_k ($k = 1, 2, \ldots, P$) so that $y = f(x_1, x_2, \ldots, x_P)$. Hence, N samples ($i = 1, 2, \ldots, N$) for each model parameter will produce a set of P sample vectors X_k ($1 \times N$) and an associated vector Y ($1 \times N$) of output values. Then, the partial rank correlation coefficients for each parameter (R_{X_kY}) are calculated as follows (Marino et al., 2008):

$$R_{X_kY} = \frac{cov(X_k, Y)}{\sqrt{Var\,(X_k)Var(Y)}} = \frac{\sum_{i=1}^{N}(x_{ik} - \bar{x})(y_i - \bar{y})}{\sqrt{\sum_{i=1}^{N}(x_{ik} - \bar{x})^2 (y_i - \bar{y})^2}} \quad (23)$$

The R values range from -1 to 1, their magnitude indicates the parameter influence, and the sign indicates whether an increase in the parameter value corresponds to an increase or decrease in the output (Helton et al., 2006). Generally, it is assumed, also in this work, that a R_{XY} values between -0.1 and 0.1 ($-0.1 < R_{XY} < 0.1$) reflect a poor level of importance of a parameter.

The combined LHS-PRCC procedure is fully described elsewhere (Marino et al., 2008), but generally involves (i) sampling of the parameter space, (ii) obtaining model output for each set of sampled parameters, (iii) ranking parameter and output values and replacing their original values with their ranks, and (iv) calculating the R_{XY} for each input parameter.

Table 3
The goodness of fit for the model adjusted to simulated data.

Goodness of fit	RMSE (mM)		R^2	
Case study	Dosage	No dosage	Dosage	No dosage
TOC	0.005	0.0008	0.998	0.999
H_2O_2	0.029	0.017	0.999	0.999
O_2	0.013	0.005	0.997	0.999

In regard to the model output, different options are possible, and a decision is required. The model produces many different calculated values that need to be pondered and/or aggregated to produce a reduced and comprehensive set of output values Y. The option in this work is the summation of the square errors, which be considered independently for the three process variables that are experimentally monitored (TOC, H_2O_2, and O_2):

$$Y1 = \sum_i \left(\widehat{[TOC]}_i - [TOC]_i \right)^2 \quad (24)$$

$$Y2 = \sum_j \left(\widehat{[H_2O_2]}_j - [H_2O_2]_j \right)^2 \quad (25)$$

$$Y3 = \sum_k \left(\widehat{[O_2]}_k - [O_2]_k \right)^2 \quad (26)$$

This choice favors the fidelity of the model to the available experimental data but would be open to discussion in other situations (e.g. an economic output in case of further using the model for optimization).

GSA is implemented in Simulink Design Optimization software using 150 samples obtained by LHS and all experimental data sets provided by Yu et al., 2020. Finally, the results ($R_{X_{kr}Y_r}$) for each parameter are averaged accordingly. Hence the model is discussed in regard to the chances for reducing complexity.

3. Results and discussion

3.1. Model simulation, verification, and analysis

A first step aimed at verifying the procedure and providing comparative results is fitting the model to the ideal data without experimental error from the simulation of the model using the same parameter values by Cabrera Reina et al. (2012).

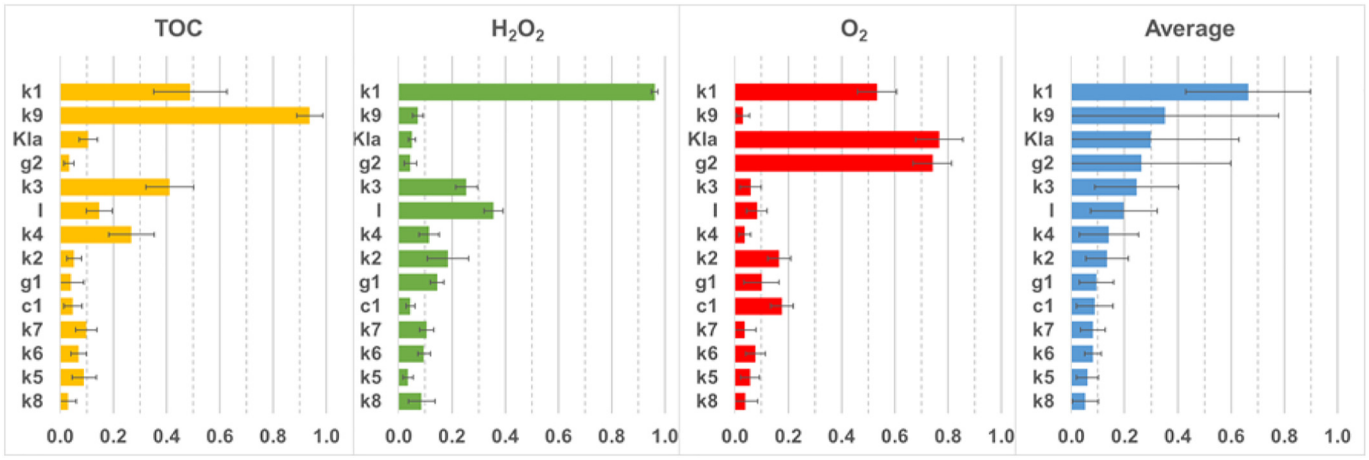

Fig. 6. Sensitivity analysis and correlation coefficients R_{XY} for all model parameters (absolute value).

Fig. 5 shows the simulations before and after parameter estimation for two cases: one with no dosage using the data provided in Table 1 and one with an additional H_2O_2 dosage profile defined by an inlet flow active from 0 to 15 min and from 45 to 60 min (Code 02).

Results show excellent agreement between the ideal data and predicted data. In the case of no dosage, the RMSE resulted in 0.0008, 0.017, 0.005 mM for TOC, H_2O_2, and O_2, respectively. In the case of dosage case, the lowest values of RMSE of 0.005, 0.029, 0. 013 mM for TOC, H_2O_2, and O_2, respectively. This is summarized in Table 3.

Thus, the quantitative results in Table 3 confirm a good tuning of the fitting method, efficient performance, and the capability to attain accurate fitting of the model to the data. Residual values and RMSE (mM) obtained with simulated data attained are much lower than the usual experimental error associated with the measurements of TOC, H_2O_2, and O_2 (Audino et al., 2019b).

3.2. Global sensitivity analysis

The robustness and complexity of the model are next analyzed via GSA, assuming independent model parameters and adopting 150 samples for each parameter using LHS-PRCC. The output is the sum of square errors between simulated and experimental data through all samples and for each measured variable (TOC, H_2O_2, and O_2).

Fig. 6 shows the corresponding averaged correlation coefficients obtained for each parameter of the photo Fenton model, sorted by its influence on the signal matching of the simulated data (obtained by LHS) to the all data sets of the experimental data for TOC, H_2O_2, and O_2 as well as the average of all those in the role of the sensitivity function. Particularly, Fig. 6 reveals that correlation coefficients for k_5, k_6 , and k_8 are below the threshold $|R_{XY}| \geq 0.10$ for all three outputs TOC, H_2O_2 and O_2, which indicates their scarce relevance to the capability of the model to fit the experimental data.

The negligible effect of k_6 and k_5 suggests that two different reactions with hydroxyl radicals (Reaction (5) with O_2 and Reaction (6) without O_2) equally compete for producing the same output. Consequently, Reactions (5) and (6) are coupled, assuming that Reaction (5) is the only reaction converting M to MX_1. Certainly, this analysis and this assumption are acceptable only in the presence of light.

On the other hand, the negligible effect of k_8 suggests that the reaction of MX_1 and R generating CO_2 (and intermediate compound MX_2) is not necessary for the model to accurately describe the delay in the conversion of M to CO_2.

These parameters with scarce influence on the model output can be omitted to reduce its complexity. Hence, they were removed, and GSA was run again without k_6 or k_8 to assess the importance of the rest of the parameters. Results are shown in Fig. 7.

Considering the same criterion ($|R_{XY}| \geq 0.10$), all the remaining parameters were revealed necessary as their corresponding $|R_{XY}|$ values were obtained greater than this threshold for at least one measured variable (TOC, H_2O_2, or O_2). Therefore, the kinetic constants (k_1, k_2, k_3,k_4,k_5,k_7,k_9, K_La), stoichiometric coefficients c_1, g_1, and g_2, in addition to operational parameter I, are finally the 12 parameters to be estimated.

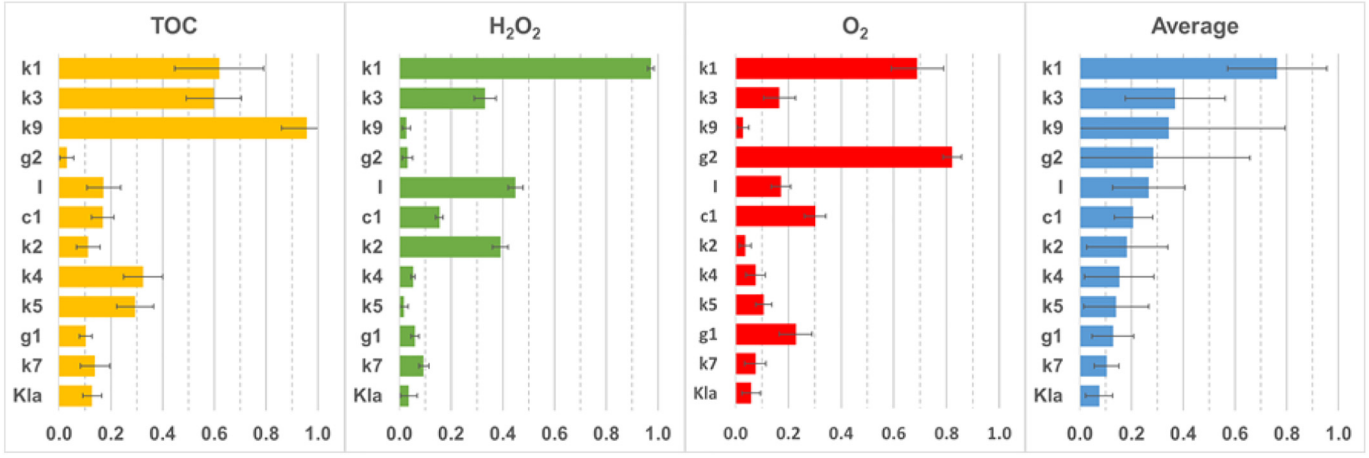

Fig. 7. Sensitivity analysis and correlation coefficients R_{XY} for all parameters of the model without k_6 and k_8 (absolute value).

Table 4
Estimation results of the kinetic parameters for Code 02 as the best fit through the first round.

Kinetic constants	Initial value	Fitted values
I (W. m^{-2})	32	29.75
$K_La(h^{-1})$	2.7	0.49
c_1	0.1	5.9
g_1	0.75	0.32
g_2	0.47	0.63
$k_1(mM^{-1}.h^{-1})$	8.81	8.07
$k_2((W.m^{-2})^{-1}.h^{-1})$	5.63	28.46
$k_3(mM^{-1}.h^{-1})$	75.8	0.97
$k_4(mM^{-1}.h^{-1})$	42,798	43,962
$k_5(mM^{-2}.h^{-1})$	2643	1113
$k_7(mM^{-1}.h^{-1})$	2865	42,133
$k_9(mM^{-1}.h^{-1})$	107	93.27
Goodness of fit	RMSE (mM)	R^2
TOC	0.010	0.99
H_2O_2	0. 200	0.96
O_2	0. 111	0.94

It is worth discussing the change in the relative significance of certain parameters after reducing the model. The most relevant variation is found for K_La, which becomes the least influential parameter. Surprisingly, K_La is revealed as the less influential parameter for explaining the behavior of dissolved oxygen.

On the one hand, the rate change of $[O_2]$ depends on (eq. 15):

- the oxygen input via dosage $[O_2]_{in}$, which is considered zero,
- the internal generation of O_2 via Reactions (3) and (4) (parameters g_1 and g_2),
- the internal consumption of O_2 via Reaction (5) (parameter c_1),
- and the diffusion of O_2 from/to the environment (parameter K_La)

On the other hand, $[O_2]$ values are close to saturation, $[O_2]^*$; the gradient $[O_2] - [O_2]^*$ is almost null, and the product is hardly affected by the value of K_La. This point is relative to the values attained by $g_1r_3 + g_2r_4 - c_1r_5$, and certainly, the same sensitivity analysis shows that g_1, g_2, and c_1 have the most significant effect on the model output after k_1. The values of g_1, g_2, and c_1 can freely combine, and effectively they do, to adjust the model response to the experimental data.

This interesting result shows that different model fittings could be able to explain the same experimental data. This is clearly connected to the prior discussion on the multiple local optima that can be encountered by the optimization algorithm and reveals that while a model can be correctly adjusted for practical purposes, further mathematical research beyond the scope of this work is required to determine the best number of model parameters and their optimal value.

3.3. Model fitting and parameter estimation

The issue when attempting the fitting of a nonlinear model to experimental data is the initial guess of the iterative optimization procedure. Fitting methods may find different sets of parameter values or may converge to local solutions, if at all (Dattner, 2015). Convergence problems and the existence of multiple optima have been detected in this work depending on the selection of the set of initial parameters values. While these problems are reported, a general solution approach is out of the scope of this work and it is not attempted. Hence, an ad-hoc heuristic is employed and presented based on using a multi-start algorithm that fits the model to individual data sets and finds a set of parameter values that applies to all the dosage profiles.

The proposed approach is summarized to execute a preliminary step with a set of initial values in the parameter space and generate a first-round fit for all assays. Then, following the strategy, the average of estimated parameter values for all the data sets are evaluated in terms of capability to predict different dosage profiles as well as acceptable goodness of fit. In the case of unacceptable fit, the new fitting round is performed starting with the best fitting results out of all data sets as the initials for the parameter search. In other words,

1. Use the reported values for the parameters (Cabrera Reina et al., 2012) as the initial values

Table 5
Estimated kinetic parameters (k_i ($mM^{-1}.h^{-1}$), k_2 ($(W.m^{-2})^{-1}.h^{-1}$), k_5 ($mM^{-2}.h^{-1}$), I ($W.m^{-2}$) and K_La (h^{-1}).

Code	I	K_La	c_1	g_1	g_2	k_1	k_2	k_3	k_4	k_5	k_7	k_9
No dosage	**221.550**	0.653	5.325	0.247	**1.007**	7.954	36.317	**68.719**	42125	1008.7	31853	96.878
0	14.859	0.426	7.157	0.248	0.694	11.638	38.077	**43.987**	35152	1045.0	85686	88.710
1	25.332	0.534	5.493	0.151	0.644	7.408	34.344	0.033	44273	1064.3	10343	84.674
2	29.751	0.493	5.902	0.319	0.633	8.073	28.458	0.971	43962	1113.0	42133	93.265
3	25.471	0.388	6.172	0.418	0.701	8.807	29.139	1.593	50899	**1694.1**	**163780**	90.318
4	28.004	0.491	5.905	0.466	0.639	8.555	22.501	0.048	44969	1118.7	51767	92.468
5	42.079	0.532	5.960	0.335	0.597	9.305	38.622	0.114	44871	1117.3	41309	90.406
7	29.595	0.511	5.897	0.321	0.621	9.650	28.423	0.155	50391	1118.5	40982	94.287
8	23.972	**1.625**	6.566	1.294	0.579	7.153	**93.918**	1.091	40703	1128.6	47280	87.024
9	57.256	0.517	5.837	0.893	0.607	8.620	52.795	9.306	48131	1080.5	53672	90.116
10	30.901	0.522	5.964	0.327	0.630	8.700	35.568	0.168	46679	1096.0	55000	89.894
11	7.159	0.440	6.428	0.904	0.606	12.423	39.853	3.440	51131	1266.6	51990	95.191
12	32.721	0.509	5.871	0.491	0.636	8.619	19.920	2.949	47142	1071.0	40721	94.046
13	69.654	0.497	5.793	0.348	0.610	9.908	19.693	9.612	47334	1119.8	41749	90.309
14	30.097	0.474	5.903	0.325	0.640	8.514	27.604	0.881	46018	1047.6	44529	89.449
Mean	44.560	0.574	6.011	0.472	0.656	9.022	36.349	9.538	45585	1139.3	53520	91.136
Median	29.751	0.509	5.903	0.335	0.633	8.620	34.344	1.091	46018	1113.0	44529	90.318
Std. Dev.	51.280	0.297	0.440	0.313	0.102	1.433	18.131	19.816	4186	164.0	34217	3.229
Confidence	28.398	0.164	0.244	0.173	0.057	0.794	10.041	10.974	2318	90.8	18949	1.788
Int.(α=0.05)	(± 64 %)	(± 29 %)	(± 4 %)	(± 37 %)	(± 9 %)	(± 9 %)	(± 28 %)	(±115%)	(± 5 %)	(± 8 %)	(± 35 %)	(± 2 %)
After discarding values beyond 3												
Mean	31.918	0.499	6.011	0.472	0.631	9.022	32.237	2.335	45585	1099.7	45644	91.136
Median	29.673	0.503	5.903	0.335	0.632	8.620	31.742	0.971	46018	1104.5	43331	90.318
Std. Dev.	15.816	0.061	0.440	0.313	0.034	1.433	8.993	3.343	4186	60.0	16090	3.229
Confidence	8.758	0.034	0.244	0.173	0.019	0.794	4.980	1.852	2318	33.2	8910	1.788
Int.(α=0.05)	(± 27 %)	(± 7 %)	(± 4 %)	(± 37 %)	(± 3 %)	(± 9 %)	(± 15 %)	(± 79 %)	(± 5 %)	(± 3 %)	(± 20 %)	(± 2 %)

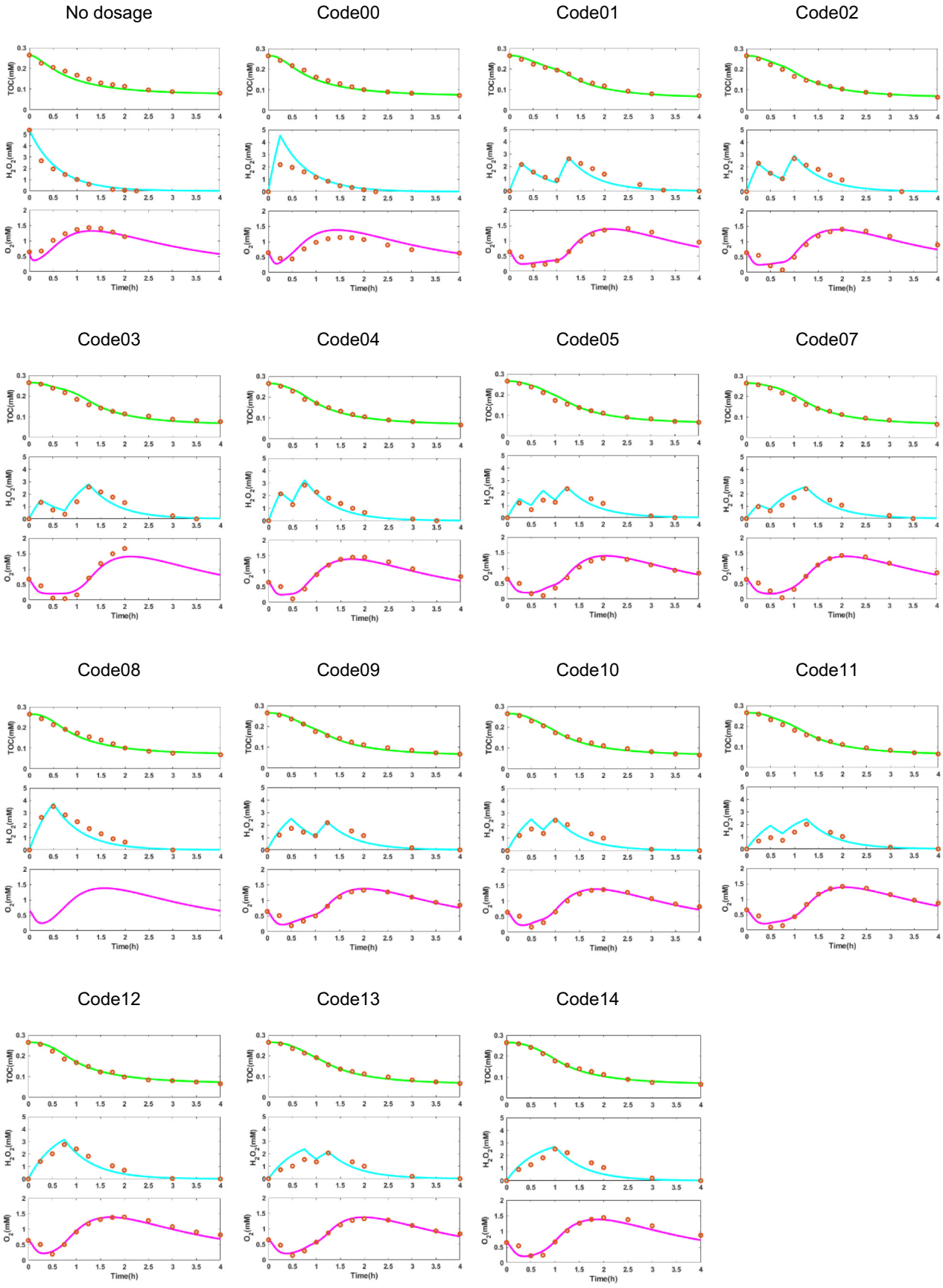

Fig. 8. Experimental data and predicted profiles in different dosage modes with final average values for the parameters.

Table 6
Root mean square error (RMSE) and coefficient of determination (R^2 Squared) for all the sets of experimental data, including those not used for model fitting (validation cases Code 06 and Code 15, which appear shadowed).

ID	ID	RMSE			R^2 Ordinary		
(Code)	(bin)	TOC (mM)	H_2O_2 (mM)	O_2 (mM)	TOC	H_2O_2	O_2
No dosage	N/A	0.0151	0.3854	0.1513	0.97	0.97	0.87
0	0000	0.0101	0.8595	0.2097	0.99	0.91	0.95
1	0001	0.0084	0.2761	0.0835	0.99	0.93	0.96
2	0010	0.0096	0.2630	0.1204	0.99	0.93	0.92
3	0011	0.0118	0.3282	0.1780	0.98	0.86	0.96
4	0100	0.0072	0.2475	0.0959	0.99	0.95	0.95
5	0101	0.0097	0.3670	0.1126	0.99	0.82	0.94
6	0110	0.0082	0.3931	0.1067	0.99	0.85	0.95
7	0111	0.0097	0.3050	0.1067	0.99	0.90	0.95
8	1000	0.0117	0.3728	-	0.97	0.95	-
9	1001	0.0078	0.3741	0.0908	0.99	0.83	0.95
10	1010	0.0077	0.4006	0.0913	0.99	0.83	0.95
11	1011	0.0091	0.4841	0.0893	0.99	0.79	0.96
12	1100	0.0087	0.3045	0.0812	0.99	0.93	0.96
13	1101	0.0064	0.4609	0.0793	0.99	0.77	0.96
14	1110	0.0065	0.4114	0.0991	0.99	0.82	0.95
15	1111	0.0089	0.2109	0.1294	0.99	0.94	0.95

2. Use the best fitting results out of all trials in the first round as initial values for the second tuning round

The parameter values reported by Cabrera Reina et al. (2012) were used as initial guesses. Next, the best fitting results (lowest RMSE) were chosen as the initial values to be used for the second round of parameter estimation.

Table 4 provides the estimation results of the kinetic parameters for Code 02 as the best fit among all reflected assays with RMSE values below 0.20 mM for TOC, H_2O_2, or O_2 using the reported values for the parameters as initials.

Table 5 displays the parameter values produced by the fitting of the model to each of the experimental data sets obtained from each dosage profile using the results obtained in the first round (see Table 4) as initial values. While the quality of the fitting is similar for all the cases, the set of values obtained for each parameter presents different distribution patterns with a very large variance in some. Parameters, k_9, c_1, k_4, k_5, g_2, k_1 present low variance (in increasing order) and, k_9 is revealed as the most certain value. Parameters, k_2, K_La, k_7, g_1, I and k_3 (in increasing order) present large variance and some disparate values. k_3 is the most fluctuating parameter.

To address this disparity, values beyond 3σ are highlighted in Table 5 (bold shadowed). These values may indicate outliers, but also suggest that fittings for No dosage, 3 and 8 may be following another pattern (which suggests in turn the determination of a different local optimum).

On the one hand, this indicates that further work may be required in regard to global optimization and attaining the same fitting in all the cases. On the other hand, identifying outliers requires a lot of caution and has no definitive criteria. From a practical point of view, the point is investigating to which extent this produces a good enough model for predicting the evolution of the process as a function of the dosage.

Hence, values beyond three standard deviations (3σ, 1 out of 370 measurements) are discarded as unlikely to have a set of 15 measurements (2,98σ was used for k_3). This allows producing more sensible data sets and average values for the next step.

Despite their variability, the average values estimated for the model parameters allow producing practical model responses matching the experimental results (Fig. 8). Fig. 8, compares the experimental data and the simulated TOC, H_2O_2, or O_2 profiles for all dosage schemes used in model fitting, and shows a qualitative image of the overall capability of the model to reproduce the measured behavior of the process, remarkably the changing trend of the H_2O_2, or O_2 profiles.

Table 6 presents the quantification of the goodness of fit for each assay. TOC values for all simulated examples were accurately predicted, and the RMSE values were lower than 0.015 mM and R^2 values were close to unity. Also, the simulation for H_2O_2 and O_2 resulted in good agreement with the experimental data, but to a lesser extent. The concentration values estimated for the monotonic evolution of TOC are accurate, within the limits of the experimental error and the precision of the measurements. Conversely, the trends estimated for the fluctuating H_2O_2 and O_2 concentration profiles (the derivatives, which may be useful for the process monitoring) follow the evolution of the experimental data, but the residual values are larger. However, these differences cause a minor influence on the practical application of the model to describe the performance of the process, which is expressed in terms of the evolution of TOC.

The average CPU time required by the multi-level method to reach convergence for one single run of parameter estimation or GSA is 20 to 30 min in a PC i7-Intel(R) Xeon(R) Silver 4114 CPU @2.20GHs 128Gb RAM. However, using Parallel Computing Toolbox™ software speeds up parameter estimation/GSA of Simulink models by distributing the simulations, and significantly reduces the total estimation run-time by 5 to 7 times.

3.4. Validation

Model validation is an important part of the study that was carried out to confirm that the model actually achieves the purpose of explaining the process dynamics under dosage schemes not included in the model fitting. Thus, the experimental data sets Code 06 and Code 15 that were not used in the calibration of model parameters were compared to the simulations obtained by setting the same dosage profiles to the model fit to the rest of the data sets. These two dosage profiles follow two different H_2O_2 supply strategies: dosing H_2O_2 continuously from 0 to 15 min and from 30 to 60 min for Code 06; and dosing H_2O_2 continuously from 0 to 75 min for Code 15 15. Fig. 9 displays the simulations and the experimental data along with their residuals for these two cases.

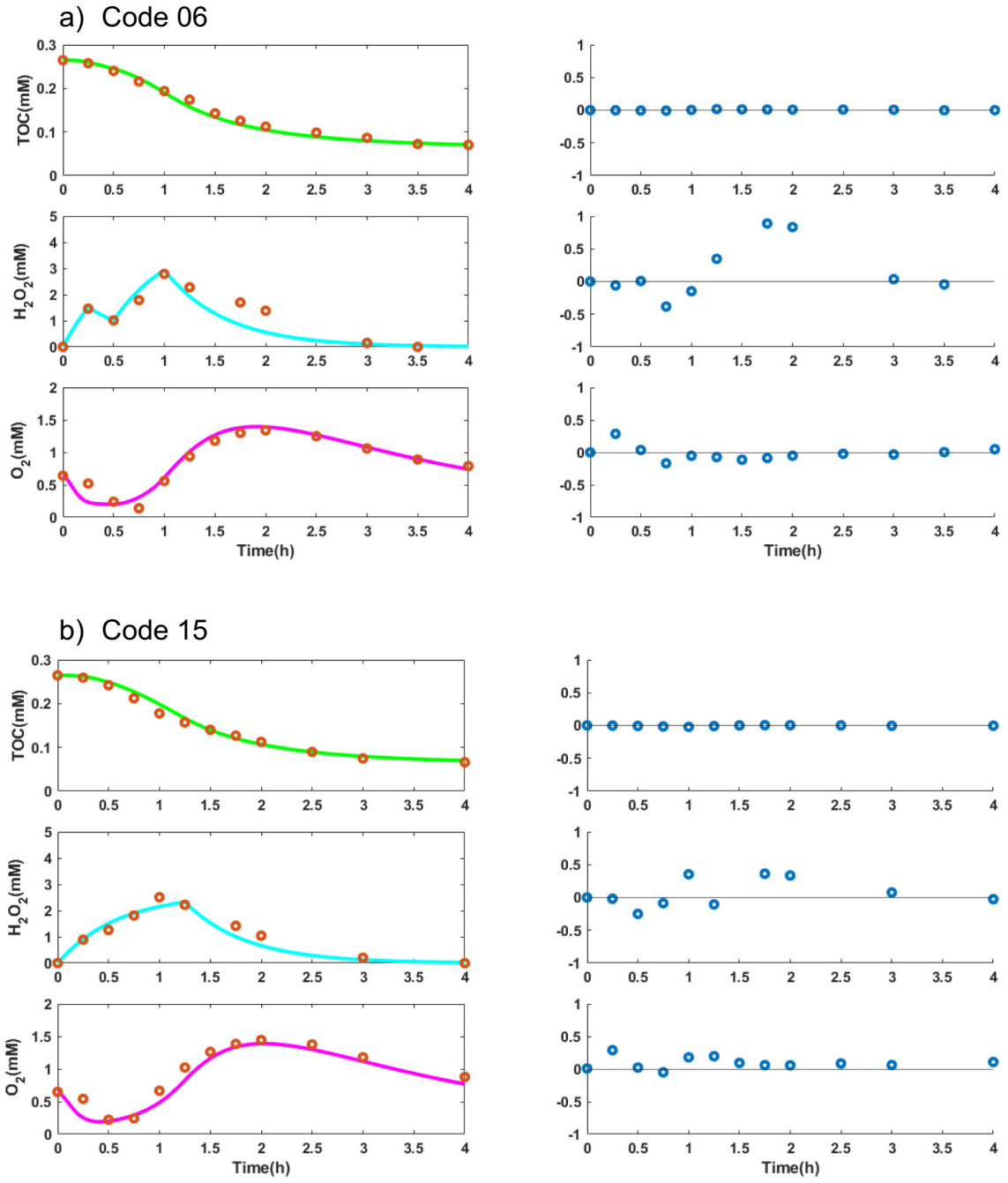

Fig. 9. Validation: experimental data (codes 06 & 15) and predicted profiles.

In both cases, the model very accurately explains the monotonic decay of the TOC concentration (RMSE<0.009 mM) as well as the convex behavior of the derivative due to the initial delay that the presence of intermediates causes in TOC response. The model also describes very well the fluctuating concentrations of hydrogen peroxide and dissolved oxygen along the 4 h reaction time. However, the residuals values for H_2O_2 and O_2 are greater than those obtained for TOC.

The quantification of the goodness of fit is also presented in Table 6. The prediction is given in the validation cases with an RMSE<0.009 mM for TOC, close to the detection error of the measurement, which is 0.02 mM. The R^2 value of 0.99 shows the good fit of the model in the case of TOC. The model is capable of describing the evolution of H_2O_2 under variable dosage with an RMSE value lower than 0.42 mM, which corresponds to 8% of the maximum H_2O_2 concentration (5.397 mM) in the reactor. Likewise, O_2 evolution was predicted properly by an RMSE <0.127 mM close to 9% the maximum O_2 concentration (1.406 mM) in the reactor.

The model validation process indicated the adequacy of the model representation of the system under study. The model and the procedure to adjust it is shown to be capable of reproducing the evolution of the reaction under diverse and variable dosage schemes and predicting future situations under new operating conditions. Hence, the tools and the methodological approach, the main contribution of this work, are ready for easily testing and assessing new dosage strategies that could be designed. On one hand, the use of a fitted model to test any given continuous time-dependent H_2O_2dosage profile would clearly provide a deeper understanding of the photo-Fenton treatment and support informed decision-making on the H_2O_2supply problem. On the other hand, the possibility of developing and fitting such a model enables the future use of model-based optimization

techniques so that the systematic exploration of alternatives could subsequently lead to determining the optimal dosage strategy for each situation.

4. Conclusions

This work contributes a novel step towards solving the optimal dosage scheme required by photo-Fenton processes. Experimental approaches are essential to providing the necessary insight into the mechanisms involved in the efficient use of hydrogen peroxide, but the exploration and assessment of all possible dosage profiles cannot be attempted experimentally. Hence, this work has presented and discussed the development, fitting, and validation of a dynamic photo-Fenton model including a flexible hydrogen peroxide supply aimed at being further exploited in determining the optimal dosage profile for a given photo-Fenton treatment. The work relies on the previous works by Cabrera Reina et al. (2012) and Audino et al. (2019a) to propose the model and uses the experimental results provided by Yu et al. (2020) to fit the model to the comprehensive set of hydrogen peroxide supply schemes.

After verifying the model with the adjustment to simulated data, a sensitivity analysis of the model fitting was performed. This analysis provided valuable insight into the nature of the model, as well as on the mathematical challenges still pending in regard to determining globally optimal fittings. Two of the reactions proposed were found to have a scarce influence on the fitting of the model, for which they were excluded. Hence, the model has been adjusted to a series of experimental data with different dosage profiles, and has been next validated using independent experimental data sets that were not used in the calibration of the model.

The validation using different dosage profiles confirmed the capacity of the model to accurately explain alternative dosage schemes, showing average errors such as RMSE<0.009 mM for TOC, RMSE<0.42 mM for H_2O_2, and RMSE <0.127 mM for O_2. Such a fidelity of the model in describing the experimental measurements can be acceptable at this point, but it will require further analysis when addressing the optimization of the dosage profile and considering the capacity of the model to accurately describe the objective function (e.g. a process economic output). Therefore, the model development is ready to address further attempts the model-based optimization of the dosage profile in subsequent investigations.

CRediT authorship contribution statement

Conceptualization; Kourosh Nasr Esfahani, Montserrat Pérez-Moya, Moisès Graells.

Data curation; Kourosh Nasr Esfahani, Montserrat Pérez-Moya, Moisès Graells.

Formal analysis; Kourosh Nasr Esfahani, Montserrat Pérez-Moya, Moisès Graells.

Funding acquisition; Kourosh Nasr Esfahani, Moisès Graells.

Investigation; Kourosh Nasr Esfahani, Montserrat Pérez-Moya, Moisès Graells.

Methodology; Kourosh Nasr Esfahani, Montserrat Pérez-Moya, Moisès Graells.

Project administration; Moisès Graells.

Resources; Software; Montserrat Pérez-Moya, Moisès Graells.

Supervision; Montserrat Pérez-Moya, Moisès Graells.

Validation; Kourosh Nasr Esfahani, Montserrat Pérez-Moya, Moisès Graells.

Visualization; Montserrat Pérez-Moya, Moisès Graells.

Roles/Writing – original draft; Kourosh Nasr Esfahani.

Writing – review & editing. Montserrat Pérez-Moya, Moisès Graells.

Declaration of competing interest

The authors declare that they have no known competing financial interests or personal relationships that could have appeared to influence the work reported in this paper.

Acknowledgments

This work was supported by the Spanish "Ministerio de Ciencia e Innovación" and the European Regional Development Fund, both funding the research Project CEPI (PID2020-116051RB-I00) which is fully acknowledged. Kourosh Nasr Esfahani appreciatively acknowledges the financial aid received by the Generalitat de Catalunya through the program FI SDUR for the Ph.D. grant (BDNS 481561).

References

Audino, F., Campanyà, G., Pérez-Moya, M., Espuña, A., Graells, M., 2019a. Systematic optimization approach for the efficient management of the photo-Fenton treatment process. Sci. Total Environ. 646, 902–913. https://doi.org/10.1016/j.scitotenv.2018.07.057.

Audino, F., Conte, L.O., Schenone, A.V., Pérez-Moya, M., Graells, M., Alfano, O.M., 2019b. A kinetic study for the Fenton and photo-Fenton paracetamol degradation in an annular photoreactor. Environ. Sci. Pollut. Res. 26, 4312–4323. https://doi.org/10.1007/s11356-018-3098-4.

Bacardit, J., Oller, I., Maldonado, M.I., Chamarro, E., Malato, S., Esplugas, S., 2007. Simple models for the control of photo-Fenton by monitoring H2O2. J. Adv. Oxid. Technol. 10, 219–228. https://doi.org/10.1515/jaots-2007-0201.

Cabrera Reina, A., Santos-Juanes Jordá, L., García Sánchez, J.L., Casas López, J.L., Sánchez Pérez, J.A., 2012. Modelling photo-Fenton process for organic matter mineralization, hydrogen peroxide consumption and dissolved oxygen evolution. Appl. Catal. B Environ. 119–120, 132–138. https://doi.org/10.1016/j.apcatb.2012.02.021.

Căilean, D., Ungureanu, F., Teodosiu, C., 2015. Homogeneous sono-Fenton process: statistical modeling and global sensitivity analysis. Int. J. Nonlinear Sci. Numer. Simul. 16, 11–21. https://doi.org/10.1515/ijnsns-2014-0051.

Campolongo, F., Cariboni, J., Saltelli, A., 2007. An effective screening design for sensitivity analysis of large models. Environ. Model. Softw. 22, 1509–1518. https://doi.org/10.1016/j.envsoft.2006.10.004.

Castillo, E., Hadi, A.S., Conejo, A., Fernández-Canteli, A., 2004. A general method for local sensitivity analysis with application to regression models and other optimization problems. Technometrics 46, 430–444. https://doi.org/10.1198/004017004000000509.

Dattner, I., 2015. A model-based initial guess for estimating parameters in systems of ordinary differential equations. Biometrics 71, 1176–1184. https://doi.org/10.1111/biom.12348.

Gulkaya, İ., Surucu, G.A., Dilek, F.B., 2006. Importance of H2O2/Fe2 + ratio in Fenton's treatment of a carpet dyeing wastewater. J. Hazard. Mater. 136, 763–769. https://doi.org/10.1016/j.jhazmat.2006.01.006.

Hamad, D., Dhib, R., Mehrvar, M., 2016. Effects of hydrogen peroxide feeding strategies on the photochemical degradation of polyvinyl alcohol. Environ. Technol. 37, 2731–2742. https://doi.org/10.1080/09593330.2016.1160959.

Helton, J.C., Johnson, J.D., Sallaberry, C.J., Storlie, C.B., 2006. Survey of sampling-based methods for uncertainty and sensitivity analysis. Reliab. Eng. Syst. Saf. 91, 1175–1209. https://doi.org/10.1016/j.ress.2005.11.017.

Latunde, T., Bamigbola, O.M., 2018. Parameter estimation and sensitivity analysis of an optimal control model for capital asset management. Adv. Fuzzy Syst. 2018, 4756520. https://doi.org/10.1155/2018/4756520.

Lu, L.A., Wang, C., Kumar, M., Lin, J.-G., 2010. Influence of pH and H2O2 dosage on the decomposition of carbofuran by the photo-Fenton process. Sustain. Environ. Res. 20, 293–297.

Lu, L.-A., Ma, Y.-S., Kumar, M., Lin, J.-G., 2011. Photochemical degradation of carbofuran and elucidation of removal mechanism. Chem. Eng. J. 166, 150–156. https://doi.org/10.1016/j.cej.2010.10.045.

Mahmoudi, N., Farhadian, M., Solaimany Nazar, A.R., Eskandari, P., Esfahani, K.N., 2021. Investigation and optimization of the performance of sono-photo-electro-Fenton process for removal of Acid Black 172 and disperse blue 56 from polluted water: comparison of the degradation activity with electro-Fenton-based processes. Int. J. Environ. Sci. Technol. https://doi.org/10.1007/s13762-021-03296-0.

Marino, S., Hogue, I.B., Ray, C.J., Kirschner, D.E., 2008. A methodology for performing global uncertainty and sensitivity analysis in systems biology. J. Theor. Biol. 254, 178–196. https://doi.org/10.1016/j.jtbi.2008.04.011.

Mousset, E., Frunzo, L., Esposito, G., Hullebusch, E.D.va, Oturan, N., Oturan, M.A., 2016. A complete phenol oxidation pathway obtained during electro-Fenton treatment and validated by a kinetic model study. Appl. Catal. B Environ. 180, 189–198. https://doi.org/10.1016/J.APCATB.2015.06.014.

Oller, I., Malato, S., Sánchez-Pérez, J.A., 2011. Combination of advanced oxidation processes and biological treatments for wastewater decontamination—a review. Sci. Total Environ. 409, 4141–4166. https://doi.org/10.1016/j.scitotenv.2010.08.061.

Ortega-Gómez, E., Moreno Úbeda, J.C., Álvarez Hervás, J.D., Casas López, J.L., Santos-Juanes Jordá, L., Sánchez Pérez, J.A., 2012. Automatic dosage of hydrogen peroxide in solar photo-Fenton plants: development of a control strategy for efficiency enhancement. J. Hazard. Mater. 237–238, 223–230. https://doi.org/10.1016/j.jhazmat.2012.08.031.

Pignatello, J., Oliveros, E., MacKay, A., 2006. Advanced oxidation processes for organic contaminant destruction based on Fenton reaction and related chemistry. Crit. Rev. Environ. Sci. Technol. 36, 1–84. https://doi.org/10.1080/10643380500326564.

Saltelli, A., Tarantola, S., Chan, K.P.-S., 1999. A quantitative model-independent method for global sensitivity analysis of model output. Technometrics 41, 39–56. https://doi.org/10.1080/00401706.1999.10485594.

Santos-Juanes, L., Sánchez, J., Casas López, J., Oller, I., Malato, S., Sánchez Pérez, J.A., 2011. Dissolved oxygen concentration: a key parameter in monitoring the photo-Fenton process. Appl. Catal. B Environ. 104, 316–323. https://doi.org/10.1016/j.apcatb.2011.03.013.

Shinozawa, Y., Heggo, D., Ookawara, S., Yoshikawa, S., 2020. Photo-Fenton degradation of carbofuran in helical tube microreactor and kinetic modeling. Ind. Eng. Chem. Res. 59, 3811–3819. https://doi.org/10.1021/acs.iecr.9b04213.

Sinnaraprasat, S., Fongsatitkul, P., 2011. Optimal condition of Fenton's reagent to enhance the alcohol production from palm oil mill effluent (POME). Environ.Asia 4, 9–16. https://doi.org/10.14456/ea.2011.12.

Spiess, A.-N., Neumeyer, N., 2010. An evaluation of R2 as an inadequate measure for nonlinear models in pharmacological and biochemical research: a Monte Carlo approach. BMC Pharmacol. 10, 6. https://doi.org/10.1186/1471-2210-10-6.

Tufail, A., Price, W., Hai, F., 2020. A critical review on advanced oxidation processes for the removal of trace organic contaminants: a voyage from individual to integrated processes. Chemosphere 260, 127460. https://doi.org/10.1016/j.chemosphere.2020.127460.

Yamal-Turbay, E., Pérez González, L., Graells, M., Pérez-Moya, M., 2014. Degradation of sulphamethazine by means of an improved photo-Fenton process involving a hydrogen peroxide systematic dosage. Environ. Technol. 35, 1695–1701. https://doi.org/10.1080/09593330.2014.880516.

Yu, X., Somoza-Tornos, A., Graells, M., Pérez-Moya, M., 2020. An experimental approach to the optimization of the dosage of hydrogen peroxide for Fenton and photo-Fenton processes. Sci. Total Environ. 743, 140402. https://doi.org/10.1016/j.scitotenv.2020.140402.